

Research article

Eesa Rahimi* and Kürşat Şendur*

Thermally controlled femtosecond pulse shaping using metasurface based optical filters

<https://doi.org/10.1515/nanoph-2017-0089>

Received September 4, 2017; revised November 17, 2017; accepted November 27, 2017

Abstract: Shaping of the temporal distribution of the ultrashort pulses, compensation of pulse deformations due to phase shift in transmission and amplification are of interest in various optical applications. To address these problems, in this study, we have demonstrated an ultra-thin reconfigurable localized surface plasmon (LSP) band-stop optical filter driven by insulator-metal phase transition of vanadium dioxide. A Joule heating mechanism is proposed to control the thermal phase transition of the material. The resulting permittivity variation of vanadium dioxide tailors spectral response of the transmitted pulse from the stack. Depending on how the pulse's spectrum is located with respect to the resonance of the band-stop filter, the thin film stack can dynamically compress/expand the output pulse span up to 20% or shift its phase up to 360°. Multi-stacked filters have shown the ability to dynamically compensate input carrier frequency shifts and pulse span variations besides their higher span expansion rates.

Keywords: optical pulse shaping; localized surface plasmons; reconfigurable optical filter; vanadium dioxide phase transition; Joule heating.

1 Introduction

Ultrashort optical pulses at the femtosecond timescale have many applications in science and technology including but not limited to light-matter interactions [1, 2], ultrafast nonlinear microscopy [3, 4], signal processing [5–7] and optical communications [8, 9]. Unprocessed ultrashort pulses from commonly used mode-locked

lasers and other sources require further refinements to be used for these purposes. In addition to shaping of the temporal distribution of the source pulses, compensation of pulse deformations in transmission and amplification is necessary for various applications. The most common method to reshape optical short pulses is through masking spectrum of spatially dispersed pulses [10]. This technique requires bulky dispersers and large spatial light modulators to be integrated to the optical pulse shaper [11]. Factors such as system and alignment complexity, bulkiness and susceptibility to vibrations restrict the functionality of spatial light modulator pulse shapers [11, 12]. Frequency-dependent reflection from Bragg gratings [12–15] and transmission through acusto-optic dispersive filters [16, 17] are other common methods of shaping ultrashort optical pulses, which have their own drawbacks, for instance, the former has narrow spectral bandwidth [12, 18], and latter is limited to pulses with kilohertz repetition rate [19]. Ring resonator and similar photonic crystal optical filters work for on-chip applications, but they also suffer from their limited bandwidth [20, 21]. Nonlinear light-matter interactions while light propagates in optical fibers [22] and bulk materials [23] are other approaches of pulse shaping.

As an alternative, light interaction with nanoscale plasmonic resonators can be employed to reshape ultrashort pulses. Engineering of temporal near-field profile for localized surface plasmons (LSPs) [24–26] or pulse shaping by reflection from featured metal films [27], transmission through sub-wavelength metallic particles [28, 29] and holes [30] are based on this technique. In this compact approach, the temporal profile of optical pulse as well as its phase and polarization are affected by resonance and dispersion properties of the plasmonic particles. In a recent study, we have shown that transmission through ultrathin resonating LSP spectrally filters the propagating pulse. The band-stop lineshape of the filter depends on the resonance strengths and its quality factors. These properties are directly related to the optical indexes and the geometry of array of particles, which can be engineered for manipulation of any specific pulse [31]. However, the lineshape of these filters is invariant once

*Corresponding authors: Eesa Rahimi and Kürşat Şendur, School of Engineering and Natural Science, Sabancı University, Istanbul, Turkey, e-mail: eesa@sabanciuniv.edu (E. Rahimi). <http://orcid.org/0000-0001-7980-4455> (E. Rahimi); sendur@sabanciuniv.edu (K. Şendur)

fabricated, and this might limit their application regardless of their compactness.

In the literature, vanadium dioxide (VO₂) is shown to dynamically tailor optical phenomena through an impact on the refractive index of the physical systems upon an external stimulus such as temperature [32], intense light [33] or charge flow [34]. It undergoes a saturating but reversible insulator to metal phase transition (IMT) in picosecond timescale [35] by heating from room temperature up to 85°C [32, 36–39]. This phase transition has been exploited for plasmonic applications through its effect on the resonance properties of LSPs [40–43]. Specifically, the lossy nature of VO₂ at high temperature in contrast with the low loss insulating properties of VO₂ at low temperature has been proposed for tailoring the performance of opto-plasmonic devices [44–47].

Here, we propose IMT in VO₂ for controlling the band-stop spectral lineshape of transmission coefficient through LSP metasurfaces for pulse shaping application. A Joule heating mechanism is proposed to control the thermal phase transition of VO₂ in an array of LSPs, and corresponding voltage-temperature equation is extracted. Temperature control of the phase transition in VO₂ is shown to manage reconfigurability of the metasurface resonance. In contrast to the works that employ VO₂ as the substrate for LSP resonance [43, 48], here, the material is only placed on the hot-spot of surface plasmons to intensify its resonance sensitivity with temperature as well as to keep the quality factor of the resonance high enough for spectral selective filtering. The reconfigurable band notch optical filters are proposed to employ two techniques, one for controlling the resonance strength and the other for adjusting the resonance frequency. We utilized a finite difference time domain solution of Maxwell equations to investigate the metasurface reconfigurability with VO₂ temperature variations. Using numerical simulations, the ability of these plasmonic filters for shaping femtosecond-scale optical pulses is studied. The effect of temperature variation on the transmitted Gaussian pulses is characterized using Fourier analysis. It is shown that the filters can provide a real-time variable pulse span compression/expansion ratios depending on how the input spectrum is located with respect to the spectral lineshape of the filter. It is also demonstrated that the filter is able to apply variable phase shift to narrow-band pulses. To provide further functionality to the optical filter, we propose stacked filters that improve pulse expansion and phase shifting abilities. The introduced pulse shaper is able to dynamically manipulate the band-stop lineshape of the filter to provide a wider control over the transmitted output pulse profile.

2 Reconfigurable metasurface

A metasurface composed of nanoparticles supporting LSPs can be employed as a band-stop spectral filter to manipulate the temporal properties of an optical transmitting wave. The band-stop lineshape can be manipulated through the particle geometry variation as shown in Ref. [31]. In this work, the lineshape adjustment is applied by controlling VO₂ material phase in the metasurface lattice through controlling its temperature. VO₂ temperature setting is obtained by Joule heating of the structure, as proposed in the schematic of Figure 1A. The structure provides a very easy to control heating mechanism, which does not restrict the optical filtering property of nano-plasmons. An applied voltage across points A and B causes a current flow in the metallic lattice, which generated resistive heat to set VO₂ temperature. The permittivity of VO₂ changes accordingly and alters the resonance of vertically oriented metallic bars with vertically polarized light. The existence of horizontal interconnects for Joule heating slightly changes this resonance by shifting its frequency; however, this part of the lattice seems almost transparent to the vertical polarized light. The thermal variation of VO₂ spectral permittivity is depicted in Figure 1B and C across the phase transition by a spline interpolation of the experimental data from the literature [49]. To avoid VO₂ permittivity ambiguities due to hysteresis [50, 51], the obtained data upon heating are reported and used in this paper. Photo-induced phase transition in VO₂ is eluded by setting the fluence of the input pulse below a certain threshold, which depends on factors such as ambient temperature and VO₂ thickness [50, 51]. Furthermore, VO₂ charge-induced phase transition does not take place here because the heating current passes thorough horizontal metallic bars but not VO₂ cubes due to the direction of applied voltage in the proposed configuration of Figure 1A.

Due to finite conductivity of the metal, applying DC voltage across terminals A and B in Figure 1A results in power loss inside the lattice in the form of heat. The overall generated heat power can be approximated by $H_{in} = (V_A - V_B)^2 / R_{equ}$, in which R_{equ} is the equivalent resistor between terminals A and B. The current flows evenly among the identical inter-terminal metallic horizontal bars; as a result, their resistances are parallel and $R_{equ} \equiv R_{hb} / n$, where R_{hb} is the resistance of each horizontal bar, n is the number of them, and terminals resistances are neglected. The resistance of each horizontal bar is given by $R_{hb} = l / (\sigma \cdot A_{cs})$, where l is the length of the bar, A_{cs} is its cross-section area, and σ is the bulk conductivity of the metal. The attached vertical metallic bars carry no

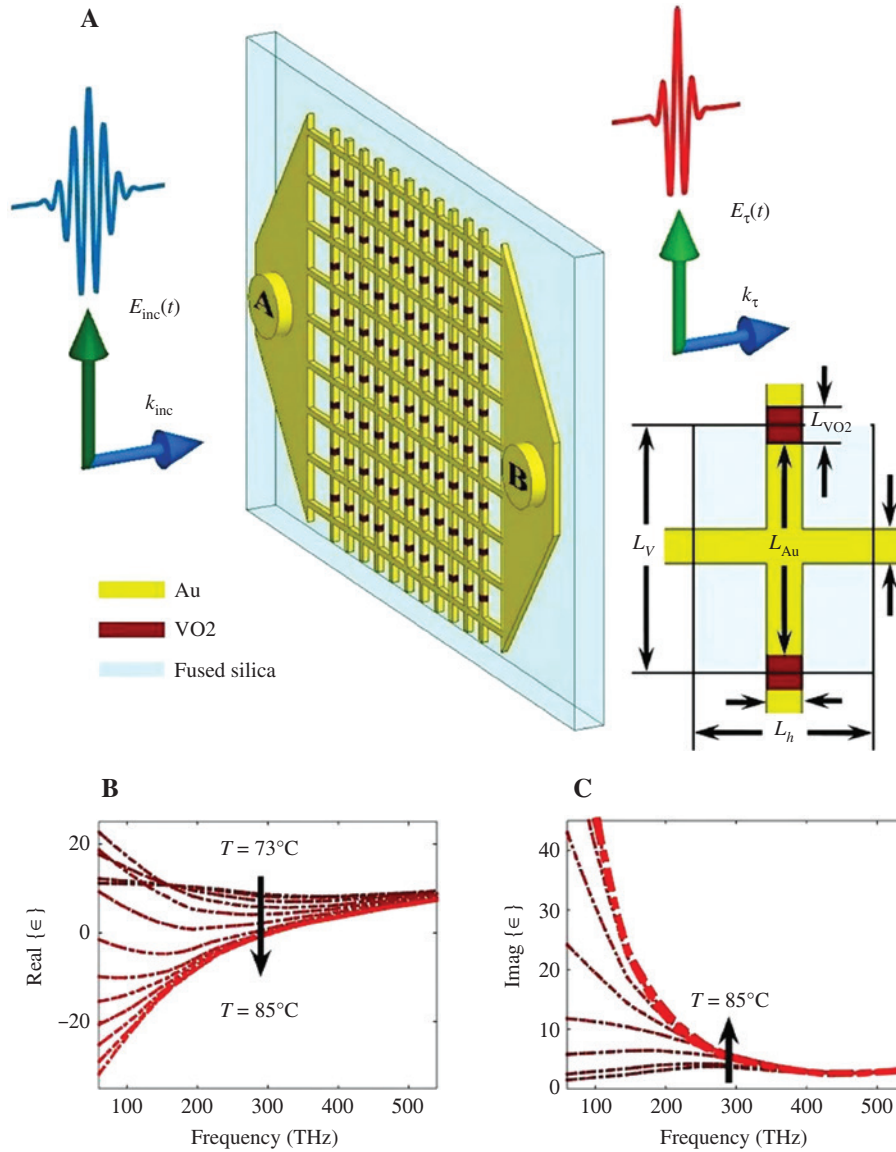


Figure 1: LSP based ultra-short pulse shaping configuration.

(A) Dynamic pulse shaping schematic by reconfigurable LSP based on insulator to metal phase transition of VO2. (B) Real and (C) imaginary parts of VO2 relative permittivity changes by temperature. The darkest red shows the material property at 73°C, and brighter reds represent the property at higher temperatures up to 85°C.

voltage-induced current and so they have negligible effects on R_{hb} . Assuming averaged natural convective cooling rate of $h_{av} = 5 \text{ W}/(\text{m}^2\text{K})$ [52] by surrounding air at T_{amb} , the heat conduction at substrate glass and the lattice metal takes place at a much higher pace for a milliliter-size structure [53], while thermal radiation to air and heat conduction through terminals and fixtures is considered negligible. Therefore, after becoming isothermal, temperature raises exponentially all over the structure to reach a steady state when the rate of lost heat by air equals the rate of generated heat in the lattice. Supposing a structure consisting of fused silica substrate of $3 \text{ mm} \times 3 \text{ mm} \times 0.5 \text{ mm}$, a gold lattice of $1 \text{ mm} \times 1 \text{ mm} \times 20 \text{ nm}$ located on top of it,

the unit cell with $L_v = 140 \text{ nm}$, $L_h = 100 \text{ nm}$, $L_{Au} = 130 \text{ nm}$, $L_{VO2} = 10 \text{ nm}$, $w = 20$ and the gold bulk conductivity of $\sigma_{Au} = 4.1 \times 10^7$ [54], one can obtain $R_{hb} = 60.1 \text{ k}\Omega$, $n = 7143$ and so $R_{equ} = 8.54 \Omega$. The resistance changes with temperature due to conductivity variation of gold are neglected here for the sake of simplicity. In the steady state, $H_{in} = H_{out} = h_{av} \cdot A_t \cdot (T_{ss} - T_{amb})$, in which A_t is the total area of the structure and T_{ss} is the steady-state temperature. Therefore,

$$T_{ss} = T_{amb} + \frac{(V_A - V_B)^2}{R_{equ} \cdot h_{av} \cdot A_t}. \tag{1}$$

Note that the filter structure is approximately isothermal and so $T_{VO2} = T_{ss}$. This equation then relates driven

voltage and VO2 temperature logically at steady state; it can be easily calibrated to set up VO2 temperature in the metasurface lattice precisely.

Thereafter, temporal response of the metasurface is extracted by calculating spectral transmission coefficient through the lattice upon normal incidence of light for different temperatures. A commercial finite difference time domain code [55] is employed to model the optical response of the proposed structure numerically. Assuming excitation of the structure with a Gaussian beam, pulse intensity (I) diminishes by $I = I_0 \exp(-2r^2/w^2)$, where I_0 is the maximum intensity, r is the distance from beam axis, and w is the beam waist. Maximum variation in intensity is inversely proportional to the beam waist. Therefore, by employing a relatively wide waist, beam variation over the metasurface lattice decreases. For very smooth spatial variation of pulse's beam over the lattice period, periodic boundaries and Floquet ports can be used to reduce the solution of this complex problem to that of a unit cell of the structure. Optical indexes of gold particle and fused silica substrate are taken from experimental data in Refs. [56] and [57], respectively. Also, it is assumed that the rear side of the substrate is covered by perfect anti-reflective coating. To ensure the accuracy of numerical analysis, mesh size in FDTD code is 10 times finer than LSP minimum skin depth at the frequency range of analysis.

The impulse response of this metasurface can comprehensively characterize its optical filtering properties, because the metasurface is time invariant in the timescale of each experiment (constant VO2 temperature in steady state) and the transmission through it is a linear function of the input pulse for the pulse fluences far below 1 mJ/cm^2 [51]. The impulse response can be calculated for a logical range of frequencies by applying a wide-band input pulse to the metasurface and measuring the transmitted output pulse. Spectral representation of the approximated transmission coefficient impulse response is then $\tau(\omega) = E_t(\omega)/E_{\text{inc}}(\omega)$, where $E_{\text{inc}}(\omega)$ indicates the spectrum of the incident input electric field ($\omega = 2\pi f$ and f is the temporal frequency), and the transmitted output electric field spectrum is $E_t(\omega)$. Once the spectral response of a metasurface is obtained, it can anticipate the transmitted optical pulse for any arbitrary input temporal profile using Fourier analysis [58].

Depending on the LSP and VO2 particles that are associated in metasurface, the thermal control can primarily manipulate either resonance depth or resonance frequency of transmission coefficient lineshape. In the former case, VO2 is employed to govern the loss rate of LSP resonances; however, in the latter case, VO2 particles add/deduct the length of the LSP resonators by transforming

interconnections of two or more LSPs to metallic/insulator. Both of the methods are illustrated by appropriate examples.

To employ VO2 as dip controller of $\tau(\omega)$, the illustrated configuration in Figure 2A with the previously mentioned dimensions can be employed. The vertically oriented LSPs are interconnected through VO2 nanoparticles that are placed on top of the transparent fused silica substrate. The longer horizontal bars do not affect the lattice resonance effectively as the pulse is vertically polarized. This structure can be fabricated using conventional electron beam lithography techniques [59, 60]. To ease electron discharge while lithography on the dielectric substrate, a very thin layer of aluminum (1–2 nm) is deposited on fused silica before coating with photoresist. This layer can be removed by a very fast wet etching at the end of fabrication process. Magnetron sputtering is recommended for VO2 deposition on fused silica after appropriate masking by photoresist. Employing this technique ensures VO2 uniformity, which plays an important role in filter performance. In magnetron sputtering, energetic ions from a gas-discharge plasma bombard a cathode containing VO2; as a result, the substrate, which functions as the anode, will be deposited by a uniform VO2 molecules coating [60].

Spectral transmission coefficient of this metasurface is calculated at different temperatures. The amplitude of $\tau(\omega)$ is shown in Figure 2B, and the corresponding phase is represented in Figure 2C. As shown in the former, in lower temperatures, the structure attenuates transmitted spectrum around a specific resonance frequency while it passes the rest of the spectrum almost unattenuated. The attenuation is caused by frequency-selective LSP resonances of free electrons inside gold nanoparticles and associated losses. Due to presence of VO2 nano-bars at the hot spot of these LSPs, the resonance is down-shifted in frequency and its quality factor is decreased [61]. However, the resonance shift by temperature variation is negligible compared to that in Ref. [61], which employs a similar material combination but different geometry to manipulate LSP extinction cross-section. Besides the geometry, the shift mainly depends on the LSP resonance range, which in this manuscript is in the mid-infrared regime. Nonetheless, VO2 permittivity has lower loss rate at near-infrared regime, which increases the sensitivity of LSP resonance to the variation of temperature. The dip in light transmission through the proposed metasurface due to resonance can be modeled by Fano-type formulation, which has been used to predict reflection from plasmonic crystals for pulse shaping purposes [27]:

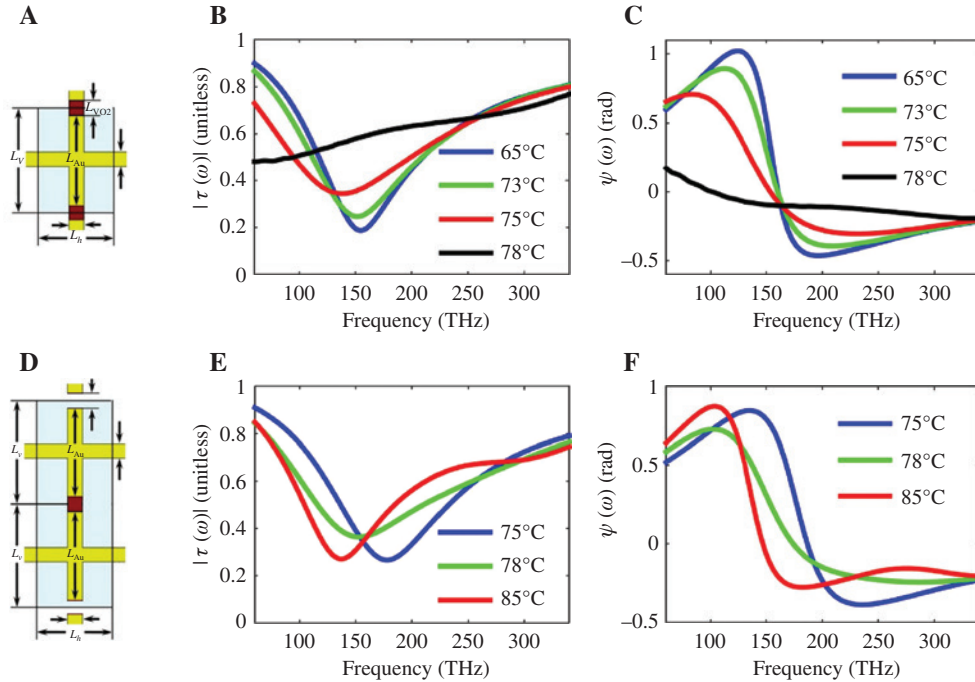


Figure 2: (A) Proposed metasurface for thermal controlling of band-stop optical filter's dip strength. Panels (B) and (C) are transmission coefficient's amplitude and phase of panel (A) in several temperatures. (D) Proposed metasurface for thermal shifting of stop resonance. Transmission coefficient's amplitude (E) and phase (F) for this metasurface in different temperatures.

$$\tau(\omega) = |\tau(\omega)| e^{j\psi(\omega)} = \tau_0 + \frac{Se^{j\phi}\Gamma}{\omega - \omega_0 + i\Gamma} \quad (2)$$

In Eq. (2), τ_0 is the nonresonant transmission amplitude, $Se^{j\phi}$ is the oscillator strength, ω_0 is the resonance angular frequency, and Γ is the frequency width of LSP resonance. The variables of this equation can be adjusted in order to fit Eq. (2) to the obtained transmission coefficient from numerical results for each temperature. By temperature increment, the band stop depth of S diminishes and the resonance frequency ω_0 shifts to the lower bands. In higher temperatures, VO2 transforms to a lossy metal, which can conduct the free electrons of gold. Consequently, surface plasmons tend to propagate rather than resonate locally. In $T=78^\circ\text{C}$, the resonance disappears and the filter passes all the spectrum with moderate attenuation. Spectral phase of transmission coefficient $\psi(\omega)$ for a sample metasurface at different temperatures is shown in Figure 2C. This phase also obeys from the phase relation of Eq. (2) once the parameters are fitted for the amplitude match. For weaker resonances in higher temperatures, filter's phase response has smoother variations. Nonetheless, for stronger resonances in lower temperatures, filter's phase response has sharper variations. The dynamics of proposed filter by temperature variation is consistent

with that in the literature although VO2 metalization may cause LSP resonance down-shift in visible range [43] instead of up-shift in infrared regime [48]. In all cases, VO2 metalization increases the loss associated to LSP resonance and the quality of the resonance decreases. Consequently, the ability of metasurface to selectively filter optical spectrum decreases.

To control the resonance frequency of $\tau(\omega)$ without considerably affecting dip strength, the shown configuration in Figure 2D can be utilized. For a unit cell of the structure, each two vertical gold bars make a resonating system while the VO2 interconnect is metallic; they become segregated resonators when VO2 is in insulator form. Figure 2E and F shows the transmission coefficient variation of such a filter with temperature for the following dimensions: $L_v=120$ nm, $L_h=100$ nm, $L_{Au}=114$ nm, $L_{VO2}=6$ nm and $w=20$. The figure points out that the resonance frequency of τ is decreased by 30% due to temperature increment from 75°C to 85°C and the general band-stop lineshape trend is approximately unchanged. While in transition between these temperatures, the resonance strength S decreases and bandwidth Γ increases because VO2 at these temperatures neither is a low-loss insulator nor is a good metal, and therefore, it adds to the loss rate of the resonators, resulting in the mentioned change of the lineshape.

3 Pulse shaping

As the proposed reconfigurable filters can tailor the spectrum of the transmitted pulse, the temporal characteristics are also changing during this process. Depending on the temporal characteristics, pulse can be shaped in different ways. In this section, we investigate the configuration in Figure 2A. The percentage (%) of half-power pulse span compression and expansion of this filter at transmission is shown in Figure 3 in different temperatures for an incident light with Gaussian temporal profile. The pulse is transform-limited, and this filter mainly affects the amplitude of its spectrum.

The red color in Figure 3 specifies the pulse compression, and the blue one shows the pulse expansion. At $T=65^\circ\text{C}$, the filter has a strong dip around 150 THz, which can compress pulse span up to 20% (widen its spectrum by selective attenuation of spectrum peak) for pulses with carrier frequencies close to this resonance. This ability decreases as the pulse span increases because the spectrum becomes narrower compared with the filter width (Γ). For pulses with carrier frequencies out of 145–165-THz band, the passing pulse through the filter undergoes expansion. The reason behind this phenomenon is that the dip at 150 THz makes the passing spectrum narrower; therefore, based on Fourier analysis, pulse width increases. The percentage of pulse expansion

is higher for shorter pulses with moderately closer carrier frequencies. At carrier frequencies far away from the filter resonance, all the spectrum that passes through it is almost unchanged and so the pulse expansion decreases. The same pattern is repeated for $T=73^\circ\text{C}$; however, due to weaker resonance strength (S) of the filter, the pulse compression/expansion ratios are decreased. Furthermore, because the filters spectral width (Γ) is expanded in this temperature, the compression frequency range is broadened to 130–170 THz. As the temperature raises to $T=75^\circ\text{C}$, the ability of the filter to expand the pulse span fades and its pulse compression ratio diminishes. Finally, at $T=78^\circ\text{C}$, the pulses pass through the filter with very negligible shape changes except for amplitude attenuation. Indeed, the intensity attenuation takes place in all the above cases due to passiveness and linearity nature of the pulse filtering; it can be as intense as $|\tau_0 + S \times \exp(j(\phi - \pi/2))|$, which is the transmission amplitude at resonance.

The performance of this pulse shaping method is comparable to fixed profile gold metasurface that has around 25% pulse compression/expansion rate in visible and near-infrared regime [31]. This ability suffices for spectrum correction on optical devices and ultrashort pulse sources such as mode-lock lasers [62]. Although acousto-optic filter may provide higher compression/expansion rates due to their phase correction capability [16, 17], their limited repetition rate and their bulkiness may restrict the

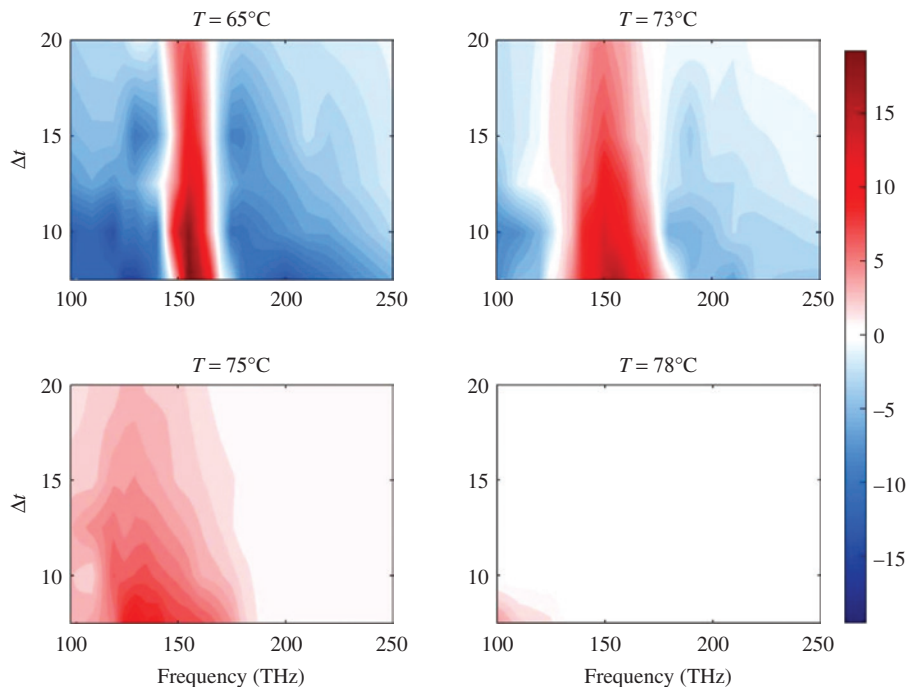


Figure 3: Half-power pulse span compression (red) and expansion (blue) percentage for various pulses with variable carrier frequencies and spans at different temperatures.

pulse modification technique for most of the applications. However, the proposed metasurface can provide ultrathin and ultracompact spectral filters for easy assembly on devices, interconnects and fibers.

On the other hand, the filter with variable dip can be a delay controller line for narrow-band pulses. In frequency ranges close to the resonance frequency, transmission coefficient amplitude has small variations. In addition, the phase is a linear function of frequency. As a result, the transmission coefficient can be approximated by $|\tau(\omega_0)|e^{j(\psi_0-\omega t_0)}$, which can make a delay to the pulse propagation for a fitted t_0 :

$$\begin{aligned} E_{\tau}(t) &= F^{-1}\{|\tau(\omega_0)|e^{j(\psi_0-\omega t_0)}E_{\text{inc}}(\omega)\} \\ &= |\tau(\omega_0)|e^{j\psi_0}E_{\text{inc}}(t-t_0) \end{aligned} \quad (3)$$

Therefore, the slope of phase $\psi(\omega)$ in this frequency band is the amount of delay time applied to the transmitted narrow-band pulse in addition to its propagation delay time. For the devised metasurface of Figure 2A, depending on the temperature of the structure, the delay time can change, as shown in Figure 4. This figure suggests that variable delay up to 8 fs can be applied to the pulse. This time delay is negligible comparing to picosecond timescale of IMT in VO₂. However, it can be employed to tune delay time between different pulses or waves. Particularly, because the period of 150-THz light is 6.67 fs, variable delay by the filter can facilitate optical phase shifting up to $360^\circ \times 8/6.67$. Even though the metasurface is not primarily designed for delay/phase adjustment, it can accommodate delay ranges that are commonly accessible by liquid crystals slabs [63].

The transmission coefficient phase is linear in a limited range of frequencies around the resonance. In this band, the transmission coefficient amplitude undergoes smooth spectral variation. To have an idea of the

amplitude variation of the filter around resonance, this property is calculated for the range of 142.5–157.5 THz (10% bandwidth) and plotted in Figure 4B. This figure shows that to apply bigger delay times to the pulse, small spectral distortion may be applied to the signal by smooth amplitude variations of the pulse up to 15%.

Monolayer metasurface can assess moderate spectral selective attenuation, which may restrict the pulse manipulation to limited pulse span changes. In order to provide versatile pulse shaping by higher spectral selective attenuations, multilayer parallel metasurfaces can be employed. However, in normal incidence of input pulse, multi-reflections between metasurfaces may cause deterioration of filter performance. In this case, by oblique incident, one can get rid of the reflection spectrum and obtain identical transmission to that of the normal incidence condition as long as the distance between the layers is set carefully to avoid reflections in the filtered light. Hence, the grating reflection modes cannot be excited for short lattice constants as it is the case here.

By setting the metasurfaces temperature of each layer differently from others, a trilayer metasurface, as shown in Figure 5A, can facilitate a fully temperature controlled pulse shaper for a range of pulses. For instance, if two top layers are filters with performance as in Figure 2A and B, also the bottom (third) layer is the filter with performance as in Figure 2C and D; by setting layers temperature $T_1:T_2:T_3$, preservation of pulse shape (widened by 90%) in different conditions is shown. If the carrier frequency of input Gaussian pulse changes, reconfigurability of the filter compensates the change to preserve the pulse shape, similarly as that seen in Figure 5B. The metasurface temperatures in degree Celsius are 73:78:85, 65:78:78 and 73:78:75 for corresponding carrier frequencies of 135 THz, 145 THz and 155 THz. If the span of input Gaussian pulse changes, filter compensates the change to preserve the pulse shape

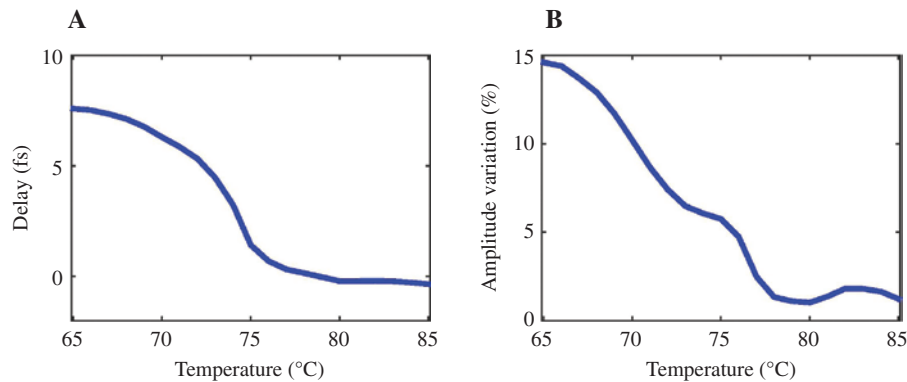


Figure 4: For the devised metasurface of Figure 2A, depending on the temperature of the structure, the delay time can change.

(A) The transmission coefficient phase slope represented in the form of a narrow-band pulse delay versus temperature at 150 THz for optical filter in Figure 2A. (B) Maximum amplitude variation of the transmission coefficient in 150 THz \pm (5%) range.

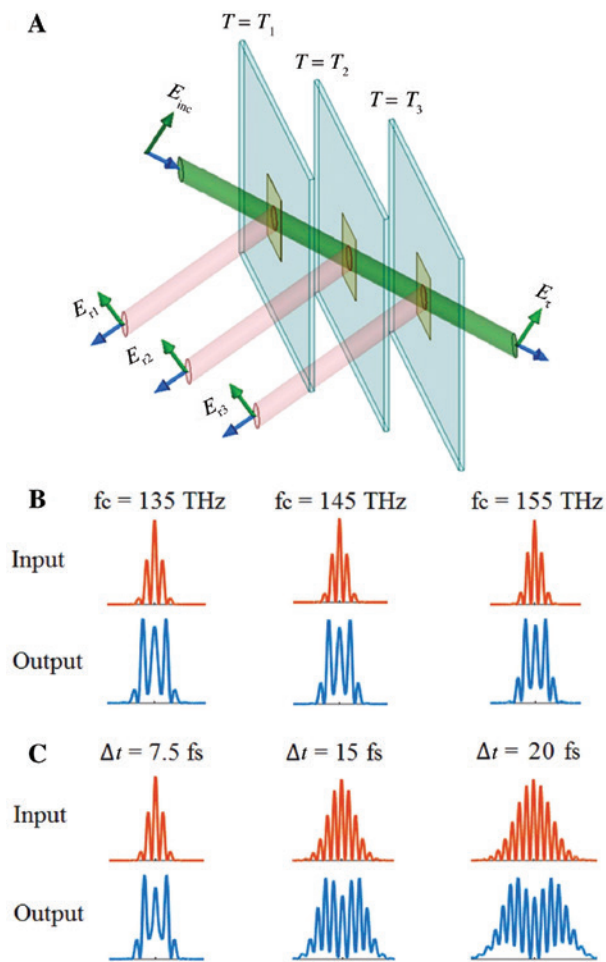


Figure 5: A trilayer metasurface can facilitate a fully temperature controlled pulse shaper for a range of pulses.

(A) Multilayer parallel metasurfaces with independent thermal controls, in which the oblique incident angle and appropriate distance between the metasurfaces avoid multi-reflections to the output. Pulse shape preservation for variable carrier frequency (B) and variable pulse span (C) using the configuration shown in (A).

and expansion rate, as illustrated in Figure 5C. The metasurface temperatures in degree Celsius are 70:78:78, 65:73:78 and 65:65:78 for corresponding pulse spans of 7.5 fs, 15 fs and 20 fs. In all the above cases, the pulse half-power span is widened by 90%. The configuration is also able to provide wider phase shifts up to $3 \times 360^\circ \times 8/6.67$ for narrow-band pulses because the transmission phase of layers is added to make a steeper overall transmission phase in the resonance region.

4 Conclusion

We have demonstrated a reconfigurable LSP-based spectral band-stop filter driven by IMT of VO₂. An appropriate

Joule heating mechanism was proposed to control the thermal phase transition of VO₂, and corresponding voltage-temperature equation was extracted. The thermally controlled phase transition of this material enables tailoring the band stop transmission response of the filter in two different ways. Either it can alter the strength of LSP resonance, which affects the filter's transmission depth, or it metalizes/demetalizes VO₂ interconnect between two LSPs and can lengthen/shorten their effective length and so alter their resonance frequency.

Using this reconfigurable optical filter, shaping femtosecond-scale optical pulses was studied. The effect of temperature variation on the transform-limited Gaussian pulse span was characterized using Fourier analysis. The filter can give a variable response depending on how the input spectrum is located, comparing the resonance of the filter. Pulse span compression/expansion ratios up to 20% were achieved by single metasurface. Moreover, the filter facilitated a flexible delay line or phase shifter to narrow-band input with less than 10% bandwidth. Then to provide much functional and versatile pulse shaper with greater abilities to compress/expand pulse span, a multilayer structure was proposed. It was shown that the metasurface temperatures can be tuned to compensate input wanted/unwanted carrier frequency shifts and pulse span variations to preserve the output pulse shape and duration.

References

- [1] Liu X, Du D, Mourou G. Laser ablation and micromachining with ultrashort laser pulses. *IEEE J Quant Electron* 1997;33:1706–16.
- [2] Di Piazza A, Müller C, Hatsagortsyan K, Keitel C. Extremely high-intensity laser interactions with fundamental quantum systems. *Rev Mod Phys* 2012;84:1177.
- [3] Squier J, Müller M. High resolution nonlinear microscopy: a review of sources and methods for achieving optimal imaging. *Rev Sci Instrum* 2001;72:2855–67.
- [4] Durst ME, Zhu G, Xu C. Simultaneous spatial and temporal focusing in nonlinear microscopy. *Opt Commun* 2008;281:1796–805.
- [5] Pelusi M, Luan F, Vo TD, et al. Photonic-chip-based radio-frequency spectrum analyser with terahertz bandwidth. *Nat Photon* 2009;3:139–43.
- [6] Krausz F, Stockman MI. Attosecond metrology: from electron capture to future signal processing. *Nat Photon* 2014;8:205–13.
- [7] Xu K. On the design and optimization of three-terminal light-emitting device in silicon CMOS technology. *J Sel Topics Quantum Electron* 2014;20:232–9.
- [8] Salehi JA, Weiner AM, Heritage JP. Coherent ultrashort light pulse code-division multiple access communication systems. *J Lightwave Technol* 1990;8:478–91.
- [9] Amiri IS, Ahmad H. Optical soliton communication using ultrashort pulses. Singapore, Springer, 2015.

- [10] Weiner AM. Ultrafast optical pulse shaping: a tutorial review. *Opt Commun* 2011;284:3669–92.
- [11] Boscolo S, Finot C. Nonlinear pulse shaping in fibres for pulse generation and optical processing. *Int J Opt* 2012;2012:1–14.
- [12] Glebov L, Smirnov V, Rotari E, et al. Volume-chirped Bragg gratings: monolithic components for stretching and compression of ultrashort laser pulses. *Opt Eng* 2014;53:051514.
- [13] Liu J-Q, Wang L-L, He M-D, et al. A wide bandgap plasmonic Bragg reflector. *Opt Express* 2008;16:4888–94.
- [14] Stepanov DY, Corena L. Bragg grating fabrication with wide range coarse and fine wavelength control. *Opt Express* 2014;22:27309–20.
- [15] Musorin A, Sharipova M, Dolgova T, Inoue M, Fedyanin A. Ultrafast Faraday rotation of slow light. *Phys Rev Applied* 2016;6:024012.
- [16] Verluise F, Laude V, Cheng Z, Spielmann C, Tournois P. Amplitude and phase control of ultrashort pulses by use of an acousto-optic programmable dispersive filter: pulse compression and shaping. *Optics Lett* 2000;25:575–7.
- [17] Kaplan D, Tournois P. Theory and performance of the acousto-optic programmable dispersive filter used for femtosecond laser pulse shaping. *Journal de Physique IV (Proceedings)* 12(5). EDP sciences, 2002, pp. 69–75.
- [18] Chauhan VCK. Pulse compression and dispersion control in ultrafast optics, PhD Diss., Georgia Institute of Technology, USA, 2011.
- [19] Steinmeyer G. A review of ultrafast optics and optoelectronics. *J Optics A Pure Appl Optics* 2002;5:R1.
- [20] Wang T-B, Wen X-W, Yin C-P, Wang H-Z. The transmission characteristics of surface plasmon polaritons in ring resonator. *Opt Express* 2009;17:24096–101.
- [21] Janipour M, Karami MA, Sofiani R, Kashani FH. A novel adjustable plasmonic filter realization by split mode ring resonators. *J Electromagn Anal Appl* 2013;5:10.
- [22] Pawłowska M, Patas A, Achazi G, Lindinger A. Parametrically shaped femtosecond pulses in the nonlinear regime obtained by reverse propagation in an optical fiber. *Opt Lett* 2012;37:2709–11.
- [23] Krebs N, Pugliesi I, Riedle E. Pulse compression of ultrashort UV pulses by self-phase modulation in bulk material. *Appl Sci* 2013;3:153–67.
- [24] Tok RU, Şendur K. Femtosecond pulse shaping using plasmonic snowflake nanoantennas. *Phys Rev A* 2011;84:033847.
- [25] Xu K, Liu H, Zhang Z. Gate-controlled diode structure based electro-optical interfaces in standard silicon-CMOS integrated circuitry. *Appl Opt* 2015;54:6420–4.
- [26] Milla M, Barho F, González-Posada F, et al. Surface-enhanced infrared absorption with Si-doped InAsSb/GaSb nano-antennas. *Opt Express* 2017;25:26651–61.
- [27] Vabishchevich PP, Shcherbakov M, Bessonov V, Dolgova T, Fedyanin A. Femtosecond pulse shaping with plasmonic crystals. *JETP Lett* 2015;101:787–92.
- [28] Shcherbakov MR, Vabishchevich PP, Shorokhov AS, et al. Ultrafast all-optical switching with magnetic resonances in nonlinear dielectric nanostructures. *Nano Lett* 2015;15:6985–90.
- [29] Sinev I, Iorsh I, Bogdanov A, et al. Polarization control over electric and magnetic dipole resonances of dielectric nanoparticles on metallic films. *Laser Photon Rev* 2016;10:799–806.
- [30] Wang Y, Qin Y, Zhang Z. Extraordinary optical transmission property of X-shaped plasmonic nanohole arrays. *Plasmonics* 2014;9:203–7.
- [31] Rahimi E, Şendur K. Femtosecond pulse shaping by ultrathin plasmonic metasurfaces. *J Opt Soc Am B* 2016;33:A1–7.
- [32] Zylbersztejn A, Mott NF. Metal-insulator transition in vanadium dioxide. *Phys Rev B* 1975;11:4383.
- [33] Becker MF, Buckman AB, Walsler RM, Lépine T, Georges P, Brun A. Femtosecond laser excitation of the semiconductor-metal phase transition in VO₂. *Appl Phys Lett* 1994;65:1507–9.
- [34] Kim H-T, Chae B-G, Youn D-H, et al. Mechanism and observation of mott transition in VO₂-based two-and three-terminal devices. *New J Phys* 2004;6:52.
- [35] Becker MF, Buckman AB, Walsler RM, Lépine T, Georges P, Brun A. Femtosecond laser excitation dynamics of the semiconductor-metal phase transition in VO₂. *J App Phys* 1996;79:2404–8.
- [36] Bianconi A, Stizza S, Bernardini R. Critical behavior of the plasmon resonance at the metal-insulator transition in VO₂. *Phys Rev B* 1981;24:4406.
- [37] Lamsal C, Ravindra N. Optical properties of vanadium oxides—an analysis. *J Mater Sci* 2013;48:6341–51.
- [38] Thompson ZJ, Stickle A, Jeong YG, et al. Terahertz-triggered phase transition and hysteresis narrowing in a nanoantenna patterned vanadium dioxide film. *Nano Lett* 2015;15:5893–8.
- [39] Muskens OL, Bergamini L, Wang Y, et al. Antenna-assisted picosecond control of nanoscale phase-transition in vanadium dioxide. *Light Sci Appl* 2016;5:e16173.
- [40] Paik T, Hong S-H, Gaubling EA, et al. Solution-processed phase-change VO₂ metamaterials from colloidal vanadium oxide (VO_x) nanocrystals. *ACS Nano* 2014;8:797–806.
- [41] Dicken MJ, Aydin K, Pryce IM, et al. Frequency tunable near-infrared metamaterials based on VO₂ phase transition. *Opt Express* 2009;17:18330–9.
- [42] Wang H, Yang Y, Wang L. Wavelength-tunable infrared metamaterial by tailoring magnetic resonance condition with VO₂ phase transition. *J Appl Phys* 2014;116:123503.
- [43] Lei DY, Appavoo K, Ligmajer F, Sonnefraud Y, Haglund RF Jr, Maier SA. Optically-triggered nanoscale memory effect in a hybrid plasmonic-phase changing nanostructure. *ACS Photon* 2015;2:1306–13.
- [44] Ferrara D, MacQuarrie E, Nag J, Kaye A, Haglund R Jr. Plasmon-enhanced low-intensity laser switching of gold: vanadium dioxide nanocomposites. *Appl Phys Lett* 2011;98:241112.
- [45] Wang L, Radue E, Kittiwatanakul S, et al. Surface plasmon polaritons in VO₂ thin films for tunable low-loss plasmonic applications. *Opt Lett* 2012;37:4335–7.
- [46] Ooi KJ, Bai P, Chu HS, Ang LK. Ultracompact vanadium dioxide dual-mode plasmonic waveguide electroabsorption modulator. *Nanophotonics* 2013;2:13–9.
- [47] Beebe M, Wang L, Madaras S, et al. Surface plasmon resonance modulation in nanopatterned Au gratings by the insulator-metal transition in vanadium dioxide films. *Opt Express* 2015;23:13222–9.
- [48] Suh J, Donev E, Ferrara D, Tetz K, Feldman L, Haglund R Jr. Modulation of the gold particle-plasmon resonance by the metal-semiconductor transition of vanadium dioxide. *J Opt A* 2008;10:055202.
- [49] Eypert C, Gaillet M. Optical characterization of VO₂ smart materials using spectroscopic ellipsometry. Japan, Horiba Scientific, 2013.
- [50] Hilton D, Prasankumar R, Fourmaux S, et al. Enhanced photosusceptibility near T_c for the light-induced insulator-to-metal phase transition in vanadium dioxide. *Phys Rev Lett* 2007;99:226401.

- [51] Pashkin A, Kübler C, Ehrke H, et al. Ultrafast insulator-metal phase transition in VO₂ studied by multiterahertz spectroscopy. *Phys Rev B* 2011;83:195120.
- [52] Bergman TL, Incropera FP, DeWitt DP, Lavine AS. *Fundamentals of heat and mass transfer*. USA, John Wiley & Sons, 2011.
- [53] Tritt TM. *Thermal conductivity: theory, properties, and applications*. USA, Springer Science & Business Media, 2005.
- [54] Serway RA, Jewett JW. *Principles of physics: a calculus-based text*, vol. 1. USA, Nelson Education, 2012.
- [55] FDTD. *Lumerical solutions*. Vancouver, BC, Canada, Inc., 2003.
- [56] Palik ED. *Handbook of optical constants of solids*, vol. 3. USA, Academic press, 1998.
- [57] Malitson I. Interspecimen comparison of the refractive index of fused silica. *J Opt Soc Am* 1965;55:1205–9.
- [58] Weiner AM. Femtosecond pulse shaping using spatial light modulators. *Rev Sci Instrum* 2000;71:1929–60.
- [59] Manfrinato VR, Zhang L, Su D, et al. Resolution limits of electron-beam lithography toward the atomic scale. *Nano Lett* 2013;13:1555–8.
- [60] Nag J, Haglund R Jr. Synthesis of vanadium dioxide thin films and nanoparticles. *J Phys Condens Matter* 2008;20:264016.
- [61] Ye J, Van Dorpe P. Plasmonic behaviors of gold dimers perturbed by a single nanoparticle in the gap. *Nanoscale* 2012;4:7205–11.
- [62] Haus HA. Mode-locking of lasers. *J Sel Topics Quantum Electron* 2000;6:1173–85.
- [63] Jullien A, Bortolozzo U, Grabielle S, Huignard J-P, Forget N, Residori S. Continuously tunable femtosecond delay-line based on liquid crystal cells. *Opt Express* 2016;24:14483–93.